Article

Radiomic and Artificial Intelligence Analysis with Textural Metrics, Morphological and Dynamic Perfusion Features Extracted by Dynamic Contrast-Enhanced Magnetic Resonance Imaging in the Classification of Breast Lesions

Roberta Fusco [1], Adele Piccirillo [2], Mario Sansone [2], Vincenza Granata [1,*], Paolo Vallone [1], Maria Luisa Barretta [1], Teresa Petrosino [1], Claudio Siani [3], Raimondo Di Giacomo [3], Maurizio Di Bonito [4], Gerardo Botti [5] and Antonella Petrillo [1]

[1] Radiology Division, Istituto Nazionale Tumori–Irccs-Fondazione G. Pascale, 80131 Naples, Italy; r.fusco@istitutotumori.na.it (R.F.); p.vallone@istitutotumori.na.it (P.V.); m.barretta@istitutotumori.na.it (M.L.B.); t.petrosino@istitutotumori.na.it (T.P.); a.petrillo@istitutotumori.na.it (A.P.)

[2] Department of Electrical Engineering and Information Technologies, Universita' Degli Studi Di Napoli Federico II, 80125 Naples, Italy; adelepiccirillo@gmail.com (A.P.); msansone@unina.it (M.S.)

[3] Senology Surgical Division, Istituto Nazionale Tumori–Irccs-Fondazione G. Pascale, 80131 Naples, Italy; c.siani@istitutotumori.na.it (C.S.); r.digiacomo@istitutotumori.na.it (R.D.G.)

[4] Pathology Division, Istituto Nazionale Tumori–Irccs-Fondazione G. Pascale, 80131 Naples, Italy; m.dibonito@istitutotumori.na.it

[5] Scientific Direction Istituto Nazionale Tumori–Irccs-Fondazione G. Pascale, 80131 Naples, Italy; g.botti@istitutotumori.na.it

* Correspondence: v.granata@istitutotumori.na.it; Tel.: +39-081-590-714; Fax: +39-081-590-3825

Abstract: Purpose: The aim of the study was to estimate the diagnostic accuracy of textural, morphological and dynamic features, extracted by dynamic contrast-enhanced magnetic resonance imaging (DCE-MRI) images, by carrying out univariate and multivariate statistical analyses including artificial intelligence approaches. Methods: In total, 85 patients with known breast lesion were enrolled in this retrospective study according to regulations issued by the local Institutional Review Board. All patients underwent DCE-MRI examination. The reference standard was pathology from a surgical specimen for malignant lesions and pathology from a surgical specimen or fine needle aspiration cytology, core or Tru-Cut needle biopsy for benign lesions. In total, 91 samples of 85 patients were analyzed. Furthermore, 48 textural metrics, 15 morphological and 81 dynamic parameters were extracted by manually segmenting regions of interest. Statistical analyses including univariate and multivariate approaches were performed: non-parametric Wilcoxon–Mann–Whitney test; receiver operating characteristic (ROC), linear classifier (LDA), decision tree (DT), k-nearest neighbors (KNN), and support vector machine (SVM) were utilized. A balancing approach and feature selection methods were used. Results: The univariate analysis showed low accuracy and area under the curve (AUC) for all considered features. Instead, in the multivariate textural analysis, the best performance (accuracy (ACC) = 0.78; AUC = 0.78) was reached with all 48 metrics and an LDA trained with balanced data. The best performance (ACC = 0.75; AUC = 0.80) using morphological features was reached with an SVM trained with 10-fold cross-variation (CV) and balanced data (with adaptive synthetic (ADASYN) function) and a subset of five robust morphological features (circularity, rectangularity, sphericity, gleaning and surface). The best performance (ACC = 0.82; AUC = 0.83) using dynamic features was reached with a trained SVM and balanced data (with ADASYN function). Conclusion: Multivariate analyses using pattern recognition approaches, including all morphological, textural and dynamic features, optimized by adaptive synthetic sampling and feature selection operations obtained the best results and showed the best performance in the discrimination of benign and malignant lesions.

Keywords: breast cancer; radiomics; artificial intelligence; classification

1. Introduction

Breast cancer is the most common cancer among women in the world; about one in eight women develop breast carcinoma during their lifetime. It is the main cause of tumor mortality and the second leading cause of death, after cardiovascular diseases. In the United States, it was estimated that 42,690 deaths (42,170 women and 520 men) from breast cancer would occur in 2020. In Italy, thirty percent of all cancers in the female population concern breasts, followed by colorectal (12%), lung (12%), thyroid (5%) and uterine body (5%) cancers. Most women diagnosed with breast cancer are over 50 years of age, but younger women can also present with cancer, with a probability of 2.4% up to 49 years of age, 5.5% from 50 to 69 years and 4.7% between 70 and 84 years of age [1,2]. In recent years, breast cancer survival rates have increased, and the number of deaths associated with this disease is steadily declining, largely due to factors such as earlier detection and personalized treatment approaches.

Screening for early diagnosis of breast cancer is of great interest, significantly increasing the patient's chances of survival. Clinical examination is the most readily available mode of diagnosis. It is a simple form of early detection, capable of diagnosing tumors of between 1 and 2 cm and bigger, depending on the location and breast size [3]. To this day, it remains the most common way in which breast cancers are first detected, normally by the affected women herself. An important role is played by mammography, introduced in the 1960s, which remains the gold standard for breast cancer screening [4]. It has many advantages: it is easy to perform, requires minimal technical set-up, is easy to standardize and it is possible to review and make direct comparisons with previous exams. Contrast-enhanced digital mammography (CEDM) is a quick, well-tolerated, relatively low-cost breast imaging technique that combines standard full-field digital mammography (FFDM) with an intravenous, low-osmolar, iodinated contrast medium. Nevertheless, the use of ionizing radiation and the inadequacy toward young women with dense tissue represent important drawbacks to this approach [5–10].

Ultrasound is an effective support examination to needle biopsy in the detection of most already-known breast cancers, as well as additional lesions in high-density tissue, and in the evaluation of tumor size and nodal status [11,12].

The emerging methodology of dynamic contrast-enhanced magnetic resonance imaging (DCE-MRI) is an important complementary diagnostic exam that has demonstrated great potential in the screening of high-risk women and dense breasts, in staging newly diagnosed breast cancer patients and in assessing therapy effects thanks to its minimal invasiveness and ability to visualize dynamic functional information, not available with conventional X-ray imaging or ultrasound. Its major advantages over mammography and ultrasound are the ability to image the entire breast as thin slices that comprise the entire breast volume and to measure variations in contrast uptake that provide information about the vascularity of the breast tissue [4,13,14].

Several studies proposed radiomic analysis for breast cancer detection and classification based on DCE-MRI, using information about lesion heterogeneity (textural features), morphological characteristics (round or irregular shape, smooth or irregular margins and tumor size) or dynamic information to quantify tumor vascularity [15–53]. It has been recognized that this problem can be addressed in a pattern recognition framework with the use of opportune features and classifiers.

This work aims to estimate the diagnostic accuracy of textural, morphological and dynamic features extracted by DCE-MRI images by carrying out univariate and multivariate statistical analyses, using artificial intelligence approaches in the classification of benign and malignant breast lesions.

2. Methods

2.1. Patient Selection

From October 2017 to April 2018, 85 patients with known breast lesions (mean age $\pm$ standard deviation of 52 ± 11 years (range 26–78)) were enrolled in this retrospective

study according to regulations issued by the local Institutional Review Board. All women gave their written informed consent for research purposes. Inclusion criteria: patient with known breast lesions, histologically proven, and patient underwent DCE-MRI examination. Exclusion criteria were breast implants, presence of non-removable drilling at the nipple, pacemakers, clips or other metal implants, pregnancy or possible pregnancy, inability to keep upright immobility during the examination, a history of metal allergy, renal disease or chemotherapy treatment at the time of imaging. In addition, women with severe claustrophobia or extreme obesity were considered unable to undergo the exam. Overall, 91 suspected breast lesions of 85 enrolled patients were analyzed. The median size of breast lesions was 4.5 cm (range 1.2–6 cm). Tumor stage was T1 or in situ in 24/56 (42.9%) malignant lesions, T2 in 5/56 (8.9%) malignant lesions and T3 in 27/56 (48.2%) malignant lesions. Grading was 2 in 20/56 (35.7%) malignant lesions and was 3 in 26/56 (64.3%) malignant lesions.

2.2. Imaging Protocol

The patients underwent imaging with a 1.5-T scanner (Magnetom Symphony; Siemens Medical System, Erlangen, Germany), equipped with a dedicated breast coil with 16 channels. Scan settings are reported in Table 1. Before the examination, each patient was placed in a prone position with both breasts fully exposed and naturally suspended. Breast MRI included turbo spin-echo T2-weighted axial images, turbo spin-echo T1-weighted fat-suppressed axial images and T1-weighted fast low-angle shot 3D coronal images. Moreover, one series before and nine series after intravenous injection of 0.1 mmol/kg body weight of a positive paramagnetic contrast material (Gd-DOTA; Dotarem, Guerbet, Roissy CdG CEDEX, France) were acquired with an interval between two successive scans of 56 s. An automatic injection system was used (Spectris Solaris EP MR, MEDRAD, Inc., Indianola, PA) and the injection flow rate was set to 2 mL/s, followed by a flush of 10 mL saline solution at the same rate. After acquisition of the dynamic series, a process of subtraction of the MR images between the post-contrast dynamic sequences and the pre-contrast one was automatically performed to emphasize the lesions with enhancement [4,13,54,55].

Table 1. Dynamic contrast-enhanced magnetic resonance imaging (DCE-MRI) scan settings.

Settings	DCE-MRI	Units
TR/TE/FA	5.08/2.39/15	ms/ms/deg
Pulse sequence	T1-weighted 3D FLASH	-
Plane	Coronal	-
FOV	500×500	mm^2
Matrix size	384×384	pixel
Pixel spacing	0.885×0.885	mm^2
Slice thickness	1.60	mm
Gap between slices	0	mm
No. of slices	128	-

2.3. Histopathological Analysis

The reference standard was pathology from a surgical specimen for malignant lesions and pathology from a surgical specimen or fine needle aspiration cytology (FNAC), core or Tru-Cut needle biopsy for benign lesions. Overall, 91 samples (35 benign and 56 malignant) of 85 patients were analyzed histopathologically. Histopathology analysis was linked to the regions identified by the radiologist upon MRI. Tumor stages were classified according to the system implemented by the American Joint Committee on Cancer staging. Ductal carcinoma in situ and invasive cancer tumors were counted as malignant lesions. All other results, including lobular carcinoma in situ, fibroadenoma, ductal hyperplasia, dysplasia, cysts, fibrosis and phyllodes tumor, were considered non-malignant lesions (Table 2).

Table 2. Number and corresponding percentage of the total benign or malignant breast lesions.

Benign (35 Lesions)	Number	Percentage Value (%)
Fibrosis	5	14.29
Ductal hyperplasia	14	40.00
Fibroadenoma	10	28.57
Dysplasia	2	5.71
Adenosis	3	8.57
Other	1	2.86
Malignant (56 Lesions)	**Number**	**Percentage Value (%)**
Infiltrating lobular carcinoma	14	25.00
Infiltrating ductal carcinoma	13	23.21
Ductal carcinoma in situ	24	42.86
Intraductal papilloma	2	3.57
Tubular carcinoma	1	1.79
Papillary carcinoma	2	3.57

2.4. Image Processing

Regions of interest (ROIs) were manually drawn slice-by-slice by two expert radiologists with 22 and 15 years of breast imaging experience, respectively; the segmentation was performed by the two radiologists first separately and then together and in accordance with each other, annotating all slices of the lesions. The margins of the breast lesions were defined on the third T1-weighted subtracted series of DCE-MRI, where contrast uptake was emphasized. Then, the mask obtained by the segmentation was used to obtain the volume of interest for each of the 9 series of DCE-MRI examination. An example is shown in Figure 1.

Figure 1. Segmentation (in red) on a single image of the third T1-weighted subtracted series: infiltrating ductal carcinoma in a 39-year-old woman.

For each volume of interest, textural, morphological and dynamic features were extracted by the volumes of interest obtained by the consensus of two radiologists. Radiomic textural, morphological and dynamic features were also extracted considering the volumes of interest obtained separately by the two radiologists.

All T1-weighted sequences of each patient were processed in MATLAB (The MathWorks, Inc., Natik, MA, USA) [56].

The Texture Toolbox of MATLAB®, which includes 48 parameters and performs texture analysis from a 2D or 3D input, was considered [57]; the textural features of this Toolbox were calculated according to the Image Biomarker Standardization Initiative [58]. The textural features include both first-order features and second-order ones. The Texture Toolbox package implements wavelet band-pass filtering, isotropic resampling, discretization length corrections and different quantization tools. The toolbox can be downloaded at https://it.mathworks.com/matlabcentral/fileexchange/51948-radiomics (accessed on 15 April 2019). A detailed description for each extracted textural feature has been provided in Supplementary Materials.

Morphological features describe and quantify the shape and structure of segmented volumes of interest. Malignant lesions may have very particular patterns of shape and specific irregularities on the borders. We considered a feature set including 15 morphological features including radial length average, entropy of radial length, irregularity, diameter, circularity, compactness, smoothness, roughness, sphericity, volume, rectangularity, surface, convexity, gleaning and curvature. A detailed description of the morphological features has been provided in Supplementary Materials.

Dynamic features measured by a time–intensity curve (TIC) describe the signal intensity, reflect tumor micro-vascularity characteristics and, in general, will tend to increase more in malignant cancer tissues than in healthy ones or less aggressive types of tumors [59,60]. Several features belonging to the dynamic category have been proposed so far in the literature [59,60] among them, 9 features were extracted voxel-by-voxel from volumes of interest using a semi-quantitative approach. For each of the 9 dynamic features, nine statistics were calculated: mean, mode, median, STD, median absolute deviation (MAD), range, kurtosis, IQR and skewness, for a total of 81 dynamic features. In Table 3, a description of the extracted dynamic features is provided.

Table 3. Description of the dynamic features.

Acronym	Description
AUC	Area under curve: total amount of contrast agent absorbed, computed with the trapezoidal approximation
AUCWIN	Area under wash-in phase
AUCWOUT	Area under wash-out phase
MSD	Maximum signal difference
ME	Maximum enhancement; it is determined by the ratio between the MSD and the signal intensity at the basal level—pre-contrast injection
WIN	Angular coefficient of linearized approximation of time–intensity curve (TIC) from time 0 to time to peak (TTP)—time elapsed since contrast injection to ME
WOUT	Angular coefficient of linearized approximation of TIC from time TPP to last time
q2	Wash-in intercept
q3	Wash-out intercept

2.5. Statistical Analysis

The statistical analyses included univariate and multivariate approaches.

2.5.1. Univariate Analysis

To assess the robustness of manual segmentation, we calculated the intra-class correlation coefficient (ICC) for the radiomic features obtained considering the two volumes of interest segmented separately by two expert radiologists.

For two-group comparisons, we used the non-parametric Wilcoxon–Mann–Whitney test for continuous variables. Receiver operating characteristic (ROC) analysis was performed. To individuate the optimal cut-off value for each feature, the Youden index was calculated. Area under the ROC curve (AUC), sensitivity (SENS), specificity (SPEC), positive predictive value

(PPV), negative predictive value (NPV) and accuracy (ACC) were obtained considering the optimal cut-off values identified by maximizing the Youden index.

2.5.2. Multivariate Analysis

Multivariate analysis was carried out using linear classifier (linear discrimination analysis—LDA), decision tree (DT), k-nearest neighbor (KNN) and support vector machine (SVM) to assess the diagnostic accuracy using all extracted metrics of textural, morphological and dynamic parameters. Configuration settings for each classifier are provided in Table 4.

Table 4. Configuration settings for each classifier.

Classifier	Configuration Settings
LDA	Covariance structure: full; optimizer options: hyperparameter options disabled
Decision tree	Fine Tree; maximum number of splits: 100; split criterion: Gini's diversity index; surrogate decision splits: off; optimizer options: hyperparameter options disabled
K-nearest neighbors	Fine KNN; number of neighbors: 100; distance metric: Euclidean; distance weight: equal; standardize data: true; optimizer options: hyperparameter options disabled
Support vector machine	Linear SVM; kernel function: linear; kernel scale: automatic; box constraint level: 1; multiclass method: one-vs-one; standardize data: true; optimizer options; hyperparameter options disabled

A brief informal description of pattern recognition approaches and of each classifier has already been discussed in a previous article [61]. The theoretical details of these classifiers can be found elsewhere [18–20,25,27–30,62–64]. Each classifier received the same set or subset of features. The analysis was made before and after a feature selection method: the robust features were selected by the least absolute shrinkage and selection operator (LASSO) method [65,66]. In the LASSO method, 10-fold cross-validation was used to select the optimal regularization parameter alpha, as the average of mean square error of each patient was the smallest. With the optimal alpha, features with a non-zero coefficient in LASSO were reserved. Note that the shrinkage requires the selection of a tuning parameter (lambda) that determines the amount of penalization. Feature selection was carried out considering the λ value with the minimum mean squared error (minMSE) [67,68].

The classification analysis was cross-validated using the 10-fold cross-validation approach, and median values of AUC, accuracy, sensitivity and specificity were obtained.

Starting with existing less-represented class samples, two techniques were used to synthesize feasible and likely data and, therefore, to help balance the classes as well as to boost the performance in terms of confusion matrix as well as overall [69,70]: the self-adaptive synthetic over-sampling (SASYNO) approach and the adaptive synthetic sampling (ADASYN) approach. The key idea of the SASYNO approach is to select neighboring minority class (benign lesions) samples based on their mutual distances and create both interpolations and extrapolations around neighboring samples for synthetic data generation. Specifically, SASYNO first identifies a population of pairwise neighboring samples from a minority class. Then, it imposes Gaussian disturbance on these identified neighboring samples to create extrapolations and, finally, generates synthetic samples by creating linear interpolations between these extrapolations [69]. The adaptive synthetic sampling (ADASYN) approach is one of the most successful advanced over-sampling approaches; it is an extension of the synthetic minority over-sampling technique (SMOTE) [70,71]. Specifically, the SMOTE [71] tackles the class imbalance problem by creating linear interpolations between randomly selected minority class samples and their neighbors of the same class. The essential idea of ADASYN is to prioritize samples near decision boundaries and to focus on these hard-to-learn minority class samples by assigning weights calculated per

sample, according to their level of difficulty in learning, as the ratio of neighbors belonging to the majority class [70,72]

The best model was chosen considering the highest area under the ROC curve and highest accuracy.

A *p* value < 0.05 was considered as significant for the univariate analysis. However, false discovery rate (FDR) adjustment according to Benjamini and Hochberg for multiple testing was considered. Statistical analyses were performed with the RStudio software [73].

3. Results

The ICC for radiomic textural, morphological and dynamic features was excellent (median value 0.86, range 0.78–0.92), demonstrating the robustness of extracted features by DCE-MRI.

Table 5 reports the diagnostic accuracy of textural, morphological and dynamic parameters in terms of AUC and *p*-value.

Table 5. List of significant textural and dynamic features with the corresponding area under curve (AUC) and *p*-values.

Textural Parameters		Symbol	AUC Values	*p*-Value
	MODE	-	0.7	0.001
First-order gray-level statistics	STANDARD DEVIATION	STD	0.7	0.001
	RANGE	-	0.73	0.000
Gray-Level Run Length Matrix (GLRLM)	Gray-Level Non-Uniformity	GLN_GLRLM	0.7	0.001
Dynamic Parameters		**Symbol**	**AUC Values**	***p*-Value**
MAD of wash-in		WIN_MAD	0.70	0.001
IQR of wash-in		WIN_IQR	0.70	0.002

Figure 2 shows ROC curve trends of significant features: mode, median, STD, range and GLN_GLRLM (Gray-Level Non-Uniformity, extracted by Gray-Level Run Length Matrix) among textural features, q2_MAD and q2_IQR (MAD and IQR calculated on q2), and WIN_MAD and WIN_IQR (MAD and IQR calculated on WIN) among dynamic ones. There are no significant morphological results (max AUC value of 0.61). Figure 3 shows the boxplots related to the above-mentioned parameters, to separate benign from malignant lesions.

As regards multivariate analysis, only the most useful results for the purposes of this work will be reported. Table 6 reports the performance achieved by the best classifiers to discriminate benign from malignant lesions.

Table 6. Performance of the best classifiers using textural, morphological and dynamic features alone and then together.

Classifier	ACC	SENS	SPEC	PPV	NPV	AUC
Performance for classifiers trained with balanced data (with ADASYN function) and all 48 textural features						
LDA	0.78	0.68	0.88	0.84	0.74	0.78
Performance for classifiers trained with balanced data (with ADASYN function) and a subset of five robust morphological features						
SVM	0.75	0.80	0.72	0.74	0.79	0.80
Performance for classifiers trained with balanced data (with ADASYN function) and a set of 21 robust dynamic features						
SVM	0.77	0.77	0.75	0.75	0.77	0.85
Performance for classifiers trained with balanced data (with ADASYN function) and a set of 37 robust features						
SVM	0.88	0.86	0.89	0.89	0.86	0.93

Note. ACC = accuracy; SENS= sensitivity; SPEC= specificity; PPV= positive predictive value; NPV = negative predictive value.
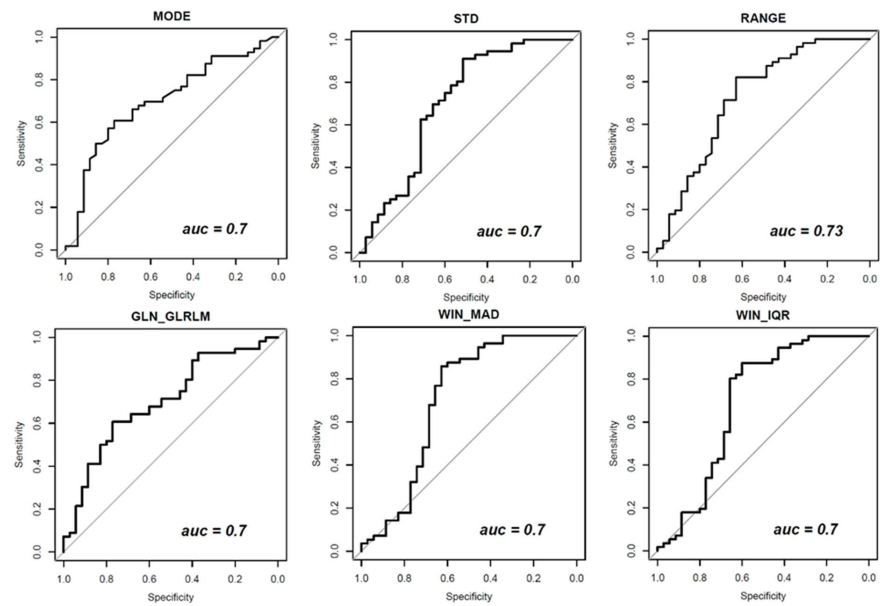
Figure 2. Receiver operating characteristic (ROC) curves of significant textural and dynamic features with AUC values.
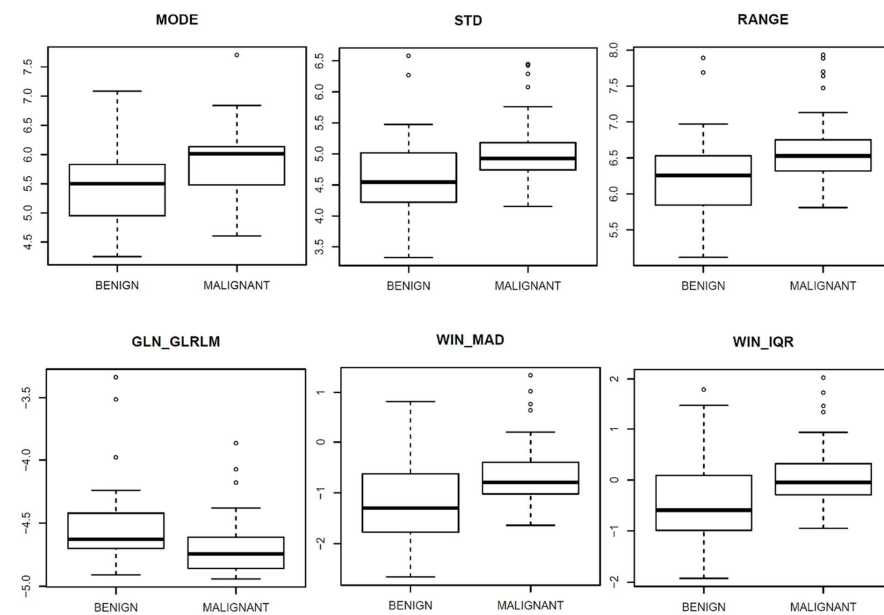

Figure 3. Boxplots of significant textural and dynamic features with AUC values.

The best performance (ACC = 0.78; SENS = 0.68; SPEC = 0.88; PPV = 0.84; NPV = 0.74; AUC = 0.78) using textural features was reached with all 48 metrics and an LDA trained with balanced data (with ADASYN function).

The best performance (ACC = 0.75; SENS = 0.80; SPEC = 0.72; PPV = 0.74; NPV = 0.79; AUC = 0.80) using morphological features was reached with an SVM trained with balanced data (with ADASYN function) and a subset of five robust morphological features. The subset of five robust morphological features included circularity (similarity of the lesion shape to a sphere), rectangularity (similarity of the lesion shape to a rectangle), sphericity (ratio between the average radial length and the standard deviation of the rays), gleaning (standard deviation of the radial lengths with respect to the radial length average) and surface (number of voxels belonging to the lesion boundary).

The best performance (ACC = 0.82; SENS = 077; SPEC = 0.88; PPV = 0.86; NPV = 0.79; AUC=0.83) using dynamic features was reached with all 81 metrics and an SVM trained with balanced data (with ADASYN function).

However, the best results overall (ACC = 0.88; SENS = 086; SPEC = 0.89; PPV = 0.89; NPV = 0.86; AUC = 0.93) were obtained considering all the features at the same time with an SVM trained with balanced data (with ADASYN function) and a subset of 37 robust radiomic features.

The subset of 37 robust radiomic features includes range, skewness, sum average, auto-correlation, GLN_GLRLM, GLV_GLRLM, LZHGE, GLV_GLSZM, convexity (ratio between the smallest volume with convex curvature that contains the lesion and its volume), irregularity (deviation of the lesion surface from the surface of a sphere), roughness (distance of each point of the center than the radial length average), gleaning, surface, MSD_KURTOSIS, MSD_SKEWNESS, MSD_IQR, ME_STD, ME_RANGE, AUC_MODE, AUC_KURTOSIS, q2_MODE, q2_MEDIAN, q2_KURTOSIS, q2_SKEWNESS, q3_SKEWNESS. WIN_MEDIAN, WIN_KURTOSIS, WIN_SKEWNESS, WOUT_MODE, WOUT_KURTOSIS, WOUT_SKEWNESS, WOUT_IQR, AUC_WIN_MODE, AUC_WIN_KURTOSIS, AUC_WIN_STD, AUC_WOUT_MODE and AUC_WOUT_KURTOSIS.

Figure 4 shows the ROC curves of the best classifiers.
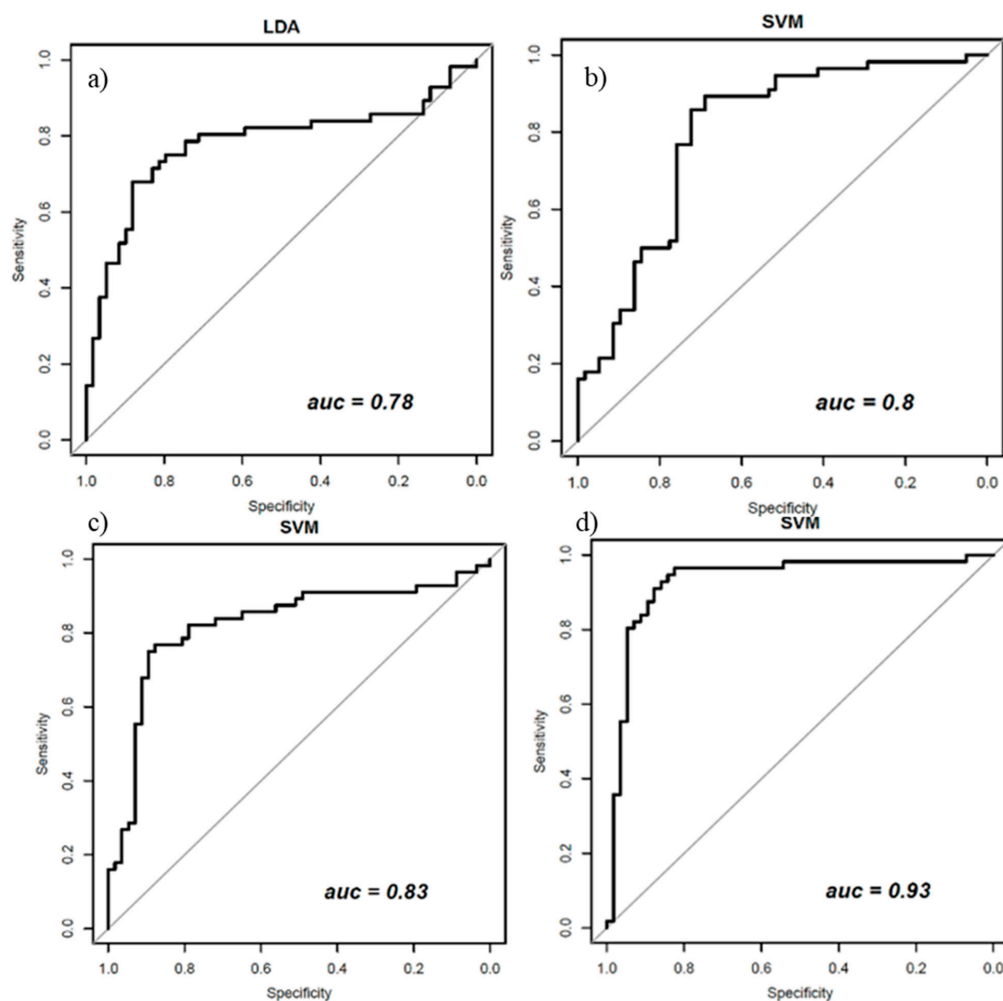
Figure 4. ROC curve of the best classifiers in (**a**) an LDA (linear discrimination analysis) using the all-balanced textural features set; in (**b**) a SVM using a subset of five robust morphological features (circularity, rectangularity, sphericity, gleaning and surface); in (**c**) an SVM using the all-balanced dynamic features set; in (**d**) an SVM with a subset of 37 robust textural, morphological and dynamic features.

4. Discussion and Conclusions

Breast MRI is the most sensitive imaging technique for breast cancer detection and the most accurate for assessment of disease extent. In recent years, many studies have addressed the problem of breast lesion classification by using several feature categories such as textural, morphological and textural features, in combination with different machine learning approaches, based on DCE-MRI images analysis [15–53]. In fact, Juntu et al. [46] reported an accuracy of 0.93 (SENS = 0.94; SPEC = 0.91) using textural features and an SVM classifier for soft tissue tumors. Mayerhoefer et al. [15] achieved an accuracy of 0.75 (SENS = 0.71; SPEC = 0.78) with an artificial neural network (ANN) classifier and using texture information from short tau inversion recovery (STIR) images for distinguishing between benign and malignant soft tissue masses. Sathya et al. [30] reported an accuracy of 0.86 (SENS = 0.88; SPEC = 0.78) using textural features and an SVM classifier to predict histologically proven malignant breast lesions. Tzacheva et al. [20] achieved an accuracy of 0.91 (SENS = 0.90; SPEC = 0.91) using static region descriptors and a neural network classifier on 14 patients to detect breast lesions. Lee et al. [48] reported a sensitivity of 0.82 and a specificity of 0.88 with dynamic features and a multilevel analysis strategy on a database of 171 breast lesions. Levman et al. [51] demonstrated statistical robustness of an SVM method that involves a reformulation of the classification/prediction process with dynamic information. In addition, Newell et al. [18] reported an accuracy of 0.93 (SPEC = 0.80; SENS = 0.97) by combining morphological and dynamic features and using an ANN classifier on a group of 216 patients. Zheng et al. [24] reported a sensitivity of 0.95 through a combination of dynamic and spatial parameters and using a linear classifier in an leave one out cross validation setting. Lastly, Agner et al. [43] yielded an accuracy of 0.90 (SENS = 0.95; SPEC = 0.82) and an AUC of 0.92 by combining texture, kinetic and morphological features on a dataset of 41 breast lesions.

In this study, we aimed to evaluate radiomic analysis with texture, morphological and dynamic features extracted by DCE-MRI images in the classification of malignant and benign breast lesions. We performed the evaluation considering both a univariate analysis and a multivariate analysis using pattern recognition approaches.

The univariate textural analysis showed statistically positive results for MODE (AUC = 0.7), STD (AUC = 0.7) and RANGE (AUC = 0.73) among first-order gray-level statistics, in addition to GLN as regards both the Gray-Level Run-Length Matrix and the Gray-Level Size Zone Matrix (AUC values of 0.70 and 0.69, respectively). As regards multivariate texture analysis, using the unbalanced dataset showed no significant results; in particular, specificity assumed very low values. After a first balancing operation (with ADASYN function), higher values of accuracy, specificity and AUC, but lower ones of sensitivity, were measured. An LDA trained with balanced data achieved the best performance with an accuracy of 0.78 and an AUC of 0.78. Using the robust textural predictors obtained by LASSO approach, no improvements were reached.

With the univariate morphological analysis, there were no significant results. With the multivariate morphology analysis, the best performance (accuracy of 0.75 and AUC of 0.80) was obtained using morphological features with an SVM trained with balanced data (with ADASYN function) and a subset of five robust morphological features including circularity, rectangularity, sphericity, gleaning and surface.

As regards the univariate dynamic analysis, higher AUC values occurred in correspondence with q2, WIN and TIC-AUC—specifically for q2_MAD (AUC = 0.68), q2_IQR (AUC = 0.68), WIN_STD (AUC = 0.68), WIN_MAD (AUC = 0.70), WIN_IQR (AUC = 0.70) and TIC-AUC_STD (AUC = 0.68). Furthermore, ME and WOUT were the least significant descriptors, with AUC values lower than 0.6.

As for the multivariate dynamic analysis, the best performance (accuracy of 0.82 and AUC of 0.83) using dynamic features was reached with an SVM trained with balanced data (with ADASYN function).

The small cohort of studied patients represents an initial finding to validate by increasing the sample size of the study in the future. The segmentation of the ROIs slice by slice

was manual, and this can be time-consuming; in fact, to analyze DCE-MRI images for each patient, the radiologists should segment them manually, spending about 2 min annotating all the slices of lesion. The future endpoint is to include in the analysis an automatic segmentation of the lesions. The radiomic analysis did not consider tumor histological differences, while the integration of texture, morphological and dynamic metrics combined with histopathology results may provide other important prognostic information for the classification of malignant breast lesions both in early and late phase. This could improve the performance in the classification problem and allow to classify breast lesions according grading and histotype. A future endpoint could be to correlate imaging metrics with clinical features such as the age of patient that could influence breast tissue with consequent radiomic effects and that could be used to classify the breast lesions according to density and BIRADS.

In conclusion, multivariate analyses using pattern recognition approaches optimized by adaptive synthetic sampling and feature selection operations obtained the best results to separate benign and malignant lesions. Among different classifiers, the SVM has proven to be the best-performing in terms of accuracy, specificity, sensitivity and ROC curve trend.

Overall, dynamic features (as a group) extracted directly from the time–intensity curve, showed the best performance. However, the best results (ACC = 0.88; AUC = 0.93) were reached by considering all characteristics of lesions (heterogeneity using textural metrics; shape and morphology features and vascularization using dynamic features), using an SVM trained with balanced data (with ADASYN function) and a subset of 37 robust features obtained with the LASSO approach.

Supplementary Materials: The following are available online at https://www.mdpi.com/2076-3417/11/4/1880/s1, Definition of textural features. Table S1: Texture features list.

Author Contributions: Each author participated sufficiently to take public responsibility for the manuscript content. R.F., A.P. (Adele Piccirillo) and M.S. performed the statistical analyses and wrote the manuscript. V.G., P.V., M.L.B., T.P., C.S., R.D.G., M.D.B., G.B. and A.P. (Antonella Petrillo) performed the investigation, defined the methodology and revised the manuscript. The authors have no conflict of interest to be disclosed. The authors confirm that the article is not under consideration for publication elsewhere. All authors have read and agreed to the published version of the manuscript.

Funding: This research received no external funding.

Institutional Review Board Statement: The study was conducted according to the guidelines of the Declaration of Helsinki, and approved by the Ethics Committee National Cancer Institute of Naples Pascale Foundation (Deliberation N. 617 of 09/08/2016).

Informed Consent Statement: All patients enrolled signed the informed consent.

Data Availability Statement: No additional data are available.

Conflicts of Interest: The authors declare that they have no known competing financial interest or personal relationships that could have appeared to influence the work reported in this paper.

References

1. AIOM. *I Numeri del Cancro in Italia*; AIOM: Milano, Italy, 2020.
2. American Cancer Society. *Breast Cancer Facts & Figures 2019–2020*; American Cancer Society Inc.: Atlanta, GA, USA, 2019; Available online: www.cancer.org/acs/groups/content/@epidemiologysurveilance/documents/document/acspc-030975.pdf (accessed on 15 November 2020).
3. Schwab, F.D.; Huang, D.J.; Schmid, S.M.; Schötzau, A.; Güth, U. Self-detection and clinical breast examination: Comparison of the two "classical" physical examination methods for the diagnosis of breast cancer. *Breast* **2015**, *24*, 90–92. [CrossRef] [PubMed]
4. Heywang-Köbrunner, S.; Viehweg, P.; Heinig, A.; Küchler, C. Contrast-enhanced MRI of the breast: Accuracy, value, controversies, solutions. *Eur. J. Radiol.* **1997**, *24*, 94–108. [CrossRef]
5. Dromain, C.; Thibault, F.; Muller, S.; Rimareix, F.; Delaloge, S.; Tardivon, A.; Balleyguier, C. Dual-energy contrast-enhanced digital mammography: Initial clinical results. *Eur. Radiol.* **2010**, *21*, 565–574. [CrossRef] [PubMed]
6. Dromain, C.; Thibault, F.; Diekmann, F.; Fallenberg, E.M.; A Jong, R.; Koomen, M.; Hendrick, R.E.; Tardivon, A.; Toledano, A. Dual-energy contrast-enhanced digital mammography: Initial clinical results of a multireader, multicase study. *Breast Cancer Res.* **2012**, *14*, R94. [CrossRef]

7. Luczynska, E.; Heinze-Paluchowska, S.; Dyczek, S.; Blecharz, P.; Ryś, J.; Reinfuss, M. Contrast-Enhanced Spectral Mammography: Comparison with Conventional Mammography and Histopathology in 152 Women. *Korean J. Radiol.* **2014**, *15*, 689–696. [CrossRef]
8. Patel, B.K.; Lobbes, M.; Lewin, J. Contrast Enhanced Spectral Mammography: A Review. *Semin. Ultrasound CT MRI* **2018**, *39*, 70–79. [CrossRef]
9. Dessouky, B.; Elsaid, N.; Shaaban, Y. Role of contrast-enhanced digital mammography in evaluation of breast lesions. *Menoufia Med. J.* **2017**, *30*, 861. [CrossRef]
10. Lewis, T.C.; Patel, B.K.; Pizzitola, V.J. Navigating contrast-enhanced digital mammography. *Appl. Radiol.* **2017**, *46*, 21–28. [CrossRef]
11. Corsetti, V.; Houssami, N.; Ghirardi, M.; Ferrari, A.; Speziani, M.; Bellarosa, S.; Remida, G.; Gasparotti, C.; Galligioni, E.; Ciatto, S. Evidence of the effect of adjunct ultrasound screening in women with mammography-negative dense breasts: Interval breast cancers at 1year follow-up. *Eur. J. Cancer* **2011**, *47*, 1021–1026. [CrossRef]
12. Hersh, M.R. Imaging the dense breast. *Appl. Radiol.* **2004**, *33*.
13. Saslow, D.; Boetes, C.; Burke, W.; Harms, S.; Leach, M.O.; Lehman, C.D.; Morris, E.; Pisano, E.; Schnall, M.; Sener, S.; et al. American Cancer Society Guidelines for Breast Screening with MRI as an Adjunct to Mammography. *CA A Cancer J. Clin.* **2007**, *57*, 75–89. [CrossRef] [PubMed]
14. Maglogiannis, I.; Zafiropoulos, E.; Anagnostopoulos, I. An intelligent system for automated breast cancer diagnosis and prognosis using SVM based classifiers. *Appl. Intell.* **2007**, *30*, 24–36. [CrossRef]
15. Mayerhoefer, M.E.; Breitenseher, M.; Amann, G.; Dominkus, M. Are signal intensity and homogeneity useful parameters for distinguishing between benign and malignant soft tissue masses on MR images? *Magn. Reson. Imaging* **2008**, *26*, 1316–1322. [CrossRef] [PubMed]
16. McLaren, C.E.; Chen, W.-P.; Nie, K.; Su, M.-Y. Prediction of Malignant Breast Lesions from MRI Features. *Acad. Radiol.* **2009**, *16*, 842–851. [CrossRef]
17. Naguib, R.N.; Adams, A.E.; Horne, C.H.; Angus, B.; Smith, A.F.; Sherbet, G.V.; Lennard, T.W. Prediction of nodal metastasis and prognosis in breast cancer: A neural model. *Anticancer Res.* **1997**, *17*, 2735–2741.
18. Newell, D.; Nie, K.; Chen, J.-H.; Hsu, C.-C.; Yu, H.J.; Nalcioglu, O.; Su, M.-Y. Selection of diagnostic features on breast MRI to differentiate between malignant and benign lesions using computer-aided diagnosis: Differences in lesions presenting as mass and non-mass-like enhancement. *Eur. Radiol.* **2009**, *20*, 771–781. [CrossRef] [PubMed]
19. Sinha, S.; Lucas-Quesada, F.A.; DeBruhl, N.D.; Sayre, J.; Farria, D.; Gorczyca, D.P.; Bassett, L.W. Multifeature analysis of Gd-enhanced MR images of breast lesions. *J. Magn. Reson. Imaging* **1997**, *7*, 1016–1026. [CrossRef] [PubMed]
20. Tzacheva, A.A.; Najarian, K.; Brockway, J.P. Breast cancer detection in gadolinium-enhanced MR images by static region descriptors and neural networks. *J. Magn. Reson. Imaging* **2003**, *17*, 337–342. [CrossRef]
21. Vergnaghi, D.; Monti, A.; Setti, E.; Musumeci, R. A use of a neural network to evaluate contrast enhancement curves in breast magnetic resonance images. *J. Digit. Imaging* **2001**, *14*, 58–59. [CrossRef]
22. Vomweg, T.W.; Buscema, P.M.; Kauczor, H.U.; Teifke, A.; Intraligi, M.; Terzi, S.; Heussel, C.P.; Achenbach, T.; Rieker, O.; Mayer, D.; et al. Improved artificial neural networks in prediction of malignancy of lesions in contrast-enhanced MR-mammography. *Med. Phys.* **2003**, *30*, 2350–2359. [CrossRef]
23. Zheng, Y.; Baloch, S.; Englander, S.; Schnall, M.D.; Shen, D. Segmentation and Classification of Breast Tumor Using Dynamic Contrast-Enhanced MR Images. *Med. Image Comput. Comput. Assist. Interv. MICCAI* **2007**, *10*, 393–401. [CrossRef]
24. Zheng, Y.; Englander, S.; Baloch, S.; Zacharaki, E.I.; Fan, Y.; Schnall, M.D.; Shen, D. STEP: Spatiotemporal enhancement pattern for MR-based breast tumor diagnosis. *Med. Phys.* **2009**, *36*, 3192–3204. [CrossRef]
25. Fukunaga, K. *Introduction to Statistical Pattern Recognition*; Elsevier: Amsterdam, The Netherlands, 1990.
26. Duda, R.O.; Hart, P.E.; Stork, D.G. *Pattern Classification*; Wiley: Hoboken, NJ, USA, 2001.
27. Theodoridis, S.; Koutroumbas, K. *Pattern Recognition*; Elsevier: Amsterdam, The Netherlands, 2003.
28. Fusco, R.; Sansone, M.; Filice, S.; Granata, V.; Catalano, O.; Amato, D.M.; Di Bonito, M.; D'Aiuto, M.; Capasso, I.; Rinaldo, M.; et al. Integration of DCE-MRI and DW-MRI Quantitative Parameters for Breast Lesion Classification. *BioMed. Res. Int.* **2015**, *2015*, 237863. [CrossRef]
29. Sathya, D.J.; Geetha, K. Mass classification in breast DCE-MR images using an artificial neural network trained via a bee colony optimization algorithm. *Science* **2013**, *39*, 294. [CrossRef]
30. Sathya, J.; Geetha, K. Experimental Investigation of Classification Algorithms for Predicting Lesion Type on Breast DCE-MR Images. *Int. J. Comput. Appl.* **2013**, *82*, 1–8. [CrossRef]
31. Ikeda, D.M.; Hylton, N.M.; Kinkel, K.; Hochman, M.G.; Kuhl, C.K.; Kaiser, W.A.; Weinreb, J.C.; Smazal, S.F.; Degani, H.; Viehweg, P.; et al. Development, standardization, and testing of a lexicon for reporting contrast-enhanced breast magnetic resonance imaging studies. *J. Magn. Reson. Imaging* **2001**, *13*, 889–895. [CrossRef]
32. Fusco, R.; Sansone, M.; Petrillo, A.; Sansone, C. A Multiple Classifier System for Classification of Breast Lesions Using Dynamic and Morphological Features in DCE-MRI. *Comput. Vis.* **2012**, *7626*, 684–692. [CrossRef]
33. Degenhard, A.; Tanner, C.; Hayes, C.; Hawkes, D.J.; O Leach, M. The UK MRI Breast Screening Study Comparison between radiological and artificial neural network diagnosis in clinical screening. *Physiol. Meas.* **2002**, *23*, 727–739. [CrossRef]
34. Castellano, G.; Bonilha, L.; Li, L.; Cendes, F. Texture analysis of medical images. *Clin. Radiol.* **2004**, *59*, 1061–1069. [CrossRef] [PubMed]

35. Haralick, R.M.; Shanmugam, K.; Dinstein, I. Textural Features for Image Classification. *IEEE Trans. Syst. Man. Cybern.* **1973**, 610–621. [CrossRef]

36. Brix, G.; Kiessling, F.; Lucht, R.; Darai, S.; Wasser, K.; Delorme, S. Microcirculation and microvasculature in breast tumors: Pharmacokinetic analysis of dynamic MR image series. *Magn. Reson. Med.* **2004**, *52*, 420–429. [CrossRef]

37. Sansone, M.; Fusco, R.; Petrillo, A.; Petrillo, M.; Bracale, M. An expectation-maximisation approach for simultaneous pixel classification and tracer kinetic modelling in dynamic contrast enhanced-magnetic resonance imaging. *Med. Biol. Eng. Comput.* **2010**, *49*, 485–495. [CrossRef]

38. Fusco, R.; Sansone, M.; Maffei, S.; Raiano, N.; Petrillo, A. Dynamic contrast-enhanced MRI in breast cancer: A comparison between distributed and compartmental tracer kinetic models. *J. Biomed. Graph. Comput.* **2012**, *2*, p23. [CrossRef]

39. Fusco, R.; Sansone, M.; Petrillo, M.; Petrillo, A. Influence of parameterization on tracer kinetic modeling in DCEMRI. *J. Med. Biol. Eng.* **2014**, *34*, 157–163. [CrossRef]

40. Fusco, R.; Sansone, M.; Sansone, C.; Petrillo, A. Segmentation and classification of breast lesions using dynamic and textural features in Dynamic Contrast Enhanced-Magnetic Resonance Imaging. In Proceedings of the 2012 25th IEEE International Symposium on Computer-Based Medical Systems (CBMS), Rome, Italy, 20–22 June 2012; IEEE: Piscataway, NJ, USA, 2012; pp. 1–4.

41. Abdolmaleki, P.; Buadu, L.D.; Murayama, S.; Murakami, J.; Hashiguchi, N.; Yabuuchi, H.; Masuda, K. Neural network analysis of breast cancer from MRI findings. *Radiat. Med.* **1998**, *15*, 283–293.

42. Abdolmaleki, P.; Buadu, L.D.; Naderimansh, H. Feature extraction and classification of breast cancer on dynamic magnetic resonance imaging using artificial neural network. *Cancer Lett.* **2001**, *171*, 183–191. [CrossRef]

43. Agner, S.C.; Soman, S.; Libfeld, E.; McDonald, M.; Thomas, K.; Englander, S.; Rosen, M.A.; Chin, D.; Nosher, J.; Madabhushi, A. Textural Kinetics: A Novel Dynamic Contrast-Enhanced (DCE)-MRI Feature for Breast Lesion Classification. *J. Digit. Imaging* **2010**, *24*, 446–463. [CrossRef]

44. Arbach, L.; Stolpen, A.; Reinhardt, J.M. Classification of breast MRI lesions using a backpropagation neural network (BNN). In Proceedings of the 2004 2nd IEEE International Symposium on Biomedical Imaging: Macro to Nano (IEEE Cat No. 04EX821), Arlington, VA, USA, 18 April 2004; IEEE: Piscataway, NJ, USA, 2005; Volume 1, pp. 253–256. [CrossRef]

45. Gilhuijs, K.G.A.; Giger, M.L.; Bick, U. Computerized analysis of breast lesions in three dimensions using dynamic magnetic-resonance imaging. *Med. Phys.* **1998**, *25*, 1647–1654. [CrossRef]

46. Juntu, J.; Sijbers, J.; De Backer, S.; Rajan, J.; Van Dyck, D. Machine learning study of several classifiers trained with texture analysis features to differentiate benign from malignant soft-tissue tumors in T1-MRI images. *J. Magn. Reson. Imaging* **2010**, *31*, 680–689. [CrossRef] [PubMed]

47. Lee, S.H.; Kim, J.H.; Park, J.S.; Jung, Y.S.; Moon, W.K. Characterizing time-intensity curves for spectral morphometric analysis of intratumoral enhancement patterns in breast DCE-MRI: Comparison between differentiation performance of temporal model parameters based on DFT and SVD. In Proceedings of the 2009 IEEE International Symposium on Biomedical Imaging: From Nano to Macro, Boston, MA, USA, 28 June–1 July 2009; pp. 65–68. [CrossRef]

48. Lee, S.H.; Kim, J.H.; Cho, N.; Park, J.S.; Yang, Z.; Jung, Y.S.; Moon, W.K. Multilevel analysis of spatiotemporal association features for differentiation of tumor enhancement patterns in breast DCE-MRI. *Med. Phys.* **2010**, *37*, 3940–3956. [CrossRef] [PubMed]

49. Leinsinger, G.; Schlossbauer, T.; Scherr, M.; Lange, O.; Reiser, M.; Wismuller, A. Cluster analysis of signal-intensity time course in dynamic breast MRI: Does unsupervised vector quantization help to evaluate small mammographic lesions? *Eur. Radiol.* **2006**, *16*, 1138–1146. [CrossRef]

50. Levman, J.; Leung, T.; Causer, P.; Plewes, D.; Martel, A.L. Classification of dynamic contrast-enhanced magnetic resonance breast lesions by support vector machines. *IEEE Trans. Med Imaging* **2008**, *27*, 688–696. [CrossRef]

51. Levman, J.; Martel, A.L. Computer-aided diagnosis of breast cancer from magnetic resonance imaging examinations by custom radial basis function vector machine. In Proceedings of the 2010 Annual International Conference of the IEEE Engineering in Medicine and Biology, Buenos Aires, Argentina, 30 August–4 September 2010; IEEE: Piscataway, NJ, USA, 2010; Volume 2010, pp. 5577–5580.

52. Lucht, R.E.; Knopp, M.V.; Brix, G. Classification of signal-time curves from dynamic MR mammography by neural networks. *Magn. Reson. Imaging* **2001**, *19*, 51–57. [CrossRef]

53. Lucht, R.; Delorme, S.; Brix, G. Neural network-based segmentation of dynamic MR mammographic images. *Magn. Reson. Imaging* **2002**, *20*, 147–154. [CrossRef]

54. Fusco, R.; Sansone, M.; Filice, S.; Petrillo, A. Breast contrast-enhanced MR imaging: Semiautomatic detection of vascular map. *Breast Cancer* **2014**, *23*, 266–272. [CrossRef]

55. Mann, R.M.; Cho, N.; Moy, L. Breast MRI: State of the Art. *Radiology* **2019**, *292*, 520–536. [CrossRef] [PubMed]

56. The MathWorks Inc. Available online: https://www.mathworks.com/ (accessed on 1 January 2019).

57. Vallières, M.; Freeman, C.R.; Skamene, S.; El Naqa, I. A radiomics model from joint FDG-PET and MRI texture features for the prediction of lung metastases in soft-tissue sarcomas of the extremities. *Phys. Med. Biol.* **2015**, *60*, 5471–5496. [CrossRef]

58. Zwanenburg, A.; Vallières, M.; Abdalah, M.A.; Aerts, H.J.W.L.; Andrearczyk, V.; Apte, A.; Ashrafinia, S.; Bakas, S.; Beukinga, R.J.; Boellaard, R.; et al. The Image Biomarker Standardization Initiative: Standardized Quantitative Radiomics for High-Throughput Im-age-based Phenotyping. *Radiology* **2020**, *295*, 328–338. [CrossRef]

59. Twellmann, T.; Saalbach, A.; Gerstung, O.; O Leach, M.; Nattkemper, T.W. Image fusion for dynamic contrast enhanced magnetic resonance imaging. *Biomed. Eng. Online* **2004**, *3*, 35. [CrossRef]

60. Wedegärtner, U.; Bick, U.; Wörtler, K.; Rummeny, E.; Bongartz, G. Differentiation between benign and malignant findings on MR-mammography: Usefulness of morphological criteria. *Eur. Radiol.* **2001**, *11*, 1645–1650. [CrossRef]

61. Fusco, R.; Sansone, M.; Filice, S.; Carone, G.; Amato, D.M.; Sansone, C.; Petrillo, A. Pattern Recognition Approaches for Breast Cancer DCE-MRI Classification: A Systematic Review. *J. Med Biol. Eng.* **2016**, *36*, 449–459. [CrossRef] [PubMed]

62. Bishop, C.M. *Pattern Recognition and Machine Learning*; Springer: Berlin/Heidelberg, Germany, 2006.

63. Cover, T.; Hart, P. Nearest neighbor pattern classification. *IEEE Trans. Inf. Theory* **1967**, *13*, 21–27. [CrossRef]

64. Tibshirani, R. The lasso Method for Variable Selection in the Cox Model. *Statist. Med.* **1997**, *16*, 385–395. [CrossRef]

65. Tibshirani, R. Regression Shrinkage and Selection Via the Lasso. *J. R. Stat. Soc. Ser. B Statist. Methodol.* **1996**, *58*, 267–288. [CrossRef]

66. James, G.; Witten, D.; Hastie, T.; Tibshirani, R. *An Introduction to Statistical Learning*; Springer: New York, NY, USA, 2013; Volume 112, p. 18.

67. Bruce, P.; Bruce, A. *Practical Statistics for Data Scientists*; O'Reilly Media, Inc.: Sebastopol, CA, USA, 2017.

68. Gu, X.; Angelov, P.P.; Soares, E.A. A self-adaptive synthetic over-sampling technique for imbalanced classification. *Int. J. Intell. Syst.* **2020**, *35*, 923–943. [CrossRef]

69. Chen, Z.; Lin, T.; Xia, X.; Xu, H.; Ding, S. A synthetic neighborhood generation based ensemble learning for the imbalanced data classification. *Appl. Intell.* **2017**, *48*, 2441–2457. [CrossRef]

70. He, H.; Bai, Y.; Garcia, E.A.; Li, S. ADASYN: Adaptive synthetic sampling approach for imbalanced learning. In Proceedings of the 2008 IEEE International Joint Conference on Neural Networks (IEEE World Congress on Computational Intelligence), Hong Kong, China, 1–6 June 2008; IEEE: Piscataway, NJ, USA, 2008; pp. 1322–1328.

71. Chawla, N.V.; Bowyer, K.W.; Hall, L.O.; Kegelmeyer, W.P. SMOTE: Synthetic minority over-sampling technique. *J. Artif. Intell. Res.* **2002**, *16*, 321–357. [CrossRef]

72. He, H.; Garcia, E.A. Learning from Imbalanced Data. *IEEE Trans. Knowl. Data Eng.* **2009**, *21*, 1263–1284. [CrossRef]

73. R-Tools Technology Inc. Available online: https://www.r-tt.com/ (accessed on 15 October 2020).